Composite Structures 261 (2021) 113593

Contents lists available at ScienceDirect

Composite Structures

journal homepage: www.elsevier.com/locate/compstruct

Mechanism of bonding of AA7075 aluminum alloy and CFRP during friction assisted joining

Francesco Lambiase [a,*], Alfonso Paoletti [a], Massimo Durante [b]

[a] University of L'Aquila, Department of Industrial and Information Engineering and Economics, via G. Gronchi 18, Zona Industriale di Pile, 67100 (AQ), Italy
[b] University of Naples Federico II, Department of Chemical, Materials and Production Engineering, P.le Tecchio 80, 80125 Naples, Italy

ARTICLE INFO

Keywords:
Friction assisted joining
Hybrid structure
Mechanical behavior
Metal composite structures

ABSTRACT

This work investigates the mechanism of bonding and the influence of the process parameters during Friction Assisted Joining of aluminum alloy AA7075 with carbon fiber reinforced PolyPhenylene Sulfide. Laser texturing was performed on the aluminum surface to promote mechanical interlocking between the metal and reinforced plastic substrates. The influence of the tool rotation speed, the plunging force, the plunging speed, and the texturing strategy on the quality of the joints was determined. The results indicated the feasibility of the process when texturized substrates were used. The mechanism of bonding was based on the mechanical interlocking between the aluminum texture and the ejected polymer matrix. Indeed, poor interaction between the texture and carbon fiber was observed regardless of the processing conditions involved. Nevertheless, the joints were characterized by high load-bearing capability (up to 10.7 kN). Besides, the process involved a short joining time (even 1 s) and required relatively low joining forces (almost 800 N).

1. Introduction

Hybrid Structures (HSs) involve parts of dissimilar materials (including metals, polymers, composites, and ceramics) to achieve the best performances from each component. This is highly demanded in several fields including transportation (automotive, aeronautical, shipbuilding), aerospace, as well as biomedical. While thermosets commonly enable higher mechanical strength, thermoplastic materials are used, especially in automotive applications, as they enable a highly flexible design of the components as well as for the capability to be processed rapidly. This permits to increase the productivity of small components. Today, the employment of reinforced thermoplastics using long and high-performance carbon fibers is continuously growing in all the transportation fields, for the issues related to end of life. The new model of the circular economy, based on the concept of 3R (Reuse, Reutilize, and Recycle), is extending the use of recyclable materials to components with high performance. These high performing materials involve more stringent issues concerning recycling as compared to not-structural components. Furthermore, in all transportation applications, hybrid constructions are highly demanded. Therefore, joining of composite materials, which are characterized by superior strength to weight ratio and chemical resistance, with lightweight metals, e.g. aluminum alloys, is becoming a challenging goal. However, since the severe differences among these materials, metals with reinforced plastics joining involves several issues. Common joining processes such as mechanical fastening and adhesive bonding are not capable to meet the demand for short joining time, high mechanical performances, low environmental impact, high automatization, etc. [1]. This is even more limiting when joining metals with carbon fiber reinforced plastics. This is driving towards the development of new joining processes that exploit the mechanical and physical properties of these two types of materials. Thermomechanical joining processes represent a viable solution when dealing with metals and thermoplastics. These processes involve an external heating source that raises the temperature at the components interface [2]. Then, the application of an external pressure enables the formation of different joining mechanisms including chemical bonding, physical bonding (mainly Van der Waals forces), and well as micro and macro interlocking [3]. Several processes have been developed so far to produce hybrid structures involving metals and plastics as well as metals and fiber-reinforced plastics. These processes may involve severe material flow during the joining processes, such as friction stir welding [4,5], friction self-riveting [6], friction-based filling stacking joining [7], injection molding [8,9], friction riveting [10,11]. On the other hand, other thermomechanical joining processes involve only a slight modification of the metal surface e.g.: laser direct

* Corresponding author at: Monteluco di Roio, 67040 (AQ), Italy.
E-mail address: francesco.lambiase@univaq.it (F. Lambiase).

https://doi.org/10.1016/j.compstruct.2021.113593
Received 2 November 2020; Revised 4 January 2021; Accepted 8 January 2021
Available online 19 January 2021

joining [12], ultrasonic joining [13–21], friction spot joining [22–28], friction lap welding [29–33], friction stir lap joining [34], as well as friction, assisted joining. This second category of processes is based on the application of an external pressure acting normal to the surface of the overlapping substrates. Then, heat is supplied to soften the polymer. These processes exploit the natural superficial irregularities (asperities and grooves), which are present on the metal surface [35]. Recent studies demonstrated that metal surface modification can dramatically increase the strength of the joints [36,37]. These surface pretreatments include surface oxidation [38–40] anodization [41,42] and above all surface structuring [43,44]. This latter process produces artificial asperities (with a height of almost 100 μm) resulting from the solidification of melted material using high power lasers. Indeed, all these processes produce a microscopic or macroscopic material flow (such as friction riveting) at relatively high temperatures. This leads to the above-mentioned joining mechanisms between the substrates. Since the first adoption of laser structuring, new joining processes have been successfully applied to produce metal-plastic hybrid structures. For example, during Friction Assisted Joining (FAJ) [45,46], a rotating tool heats the metal component by friction. The metal surface in contact with the polymer is characterized by natural or artificial asperities that sink within the polymer surface. During FAJ, the joining mechanism is based on the polymer softening and subsequent microinterlocking. Thus, the process involves moderate forces and power [47] especially if compared to friction spot joining and friction riveting. In FAJ the plunging force is mainly used to apply an external pressure. This produces the frictional heat to soften the underlying polymer. The results of several studies indicated that, the joints made by FAJ were characterized by high mechanical strength [45,46,48]. However, so far FAJ has been only applied to join metals to thermoplastic components, while no study demonstrated the feasibility of the process for joining metals to reinforced thermoplastics.

The present study aims to understand the feasibility of friction assisted joining to join aluminum AA7075 with carbon-reinforced polyphenylene sulfide. Particularly, this investigation analyzed how the presence of carbon fibers influenced the bonding mechanism, the material flow, and ultimately, how this influenced the mechanical strength of the joints. Then, the influence of the main process parameters (tool rotation speed, plunging rate, plunging load, dwell time, and depth of asperities produced by laser texturing) on the quality of the joints was determined. An instrumented CNC machine equipped with load, torque, and position sensors was adopted during the experiments. Besides, an IR thermal camera was adopted to monitor the temperature during the joining process. The quality assessment of the joints involved mechanical characterization tests and microscopic analysis.

2. Materials and methods

2.1. 2.1 materials

The experimental tests were performed on aluminum alloy AA7075 and carbon fiber reinforced PolyPhenylene Sulfide (CF-PPS). The aluminum coupons and the reinforced PPS were 3.0 mm and 2.45 mm in thickness, respectively. AA7075 is an aluminum alloy involving Zinc as the principal alloy element (typically ranging between 5.6 and 6.1%). This material is used for structural parts (especially in aeronautic and aerospace industries) as its low density and high strength, as well as high impact resistance. Aluminum sheets were cut from a unique sheet employing a laser cutting machine to a dimension of 22 × 70 mm. The main mechanical and physical characteristics of the involved materials are summarized in Table 1.

The fiber-reinforced plastic involved a thermoplastic 5-harness satin weave composite laminate supplied by TenCate Advanced Composites Company. The composite involved T300JB carbon fabric and Fortron 0214 PPS as the reinforcement and the matrix materials. The PolyPhenylene Sulfide (PPS) matrix used in the pre-preg is a semicrystalline polymer with a glass transition and melting temperature of 90 °C and 280 °C, respectively. The composite flat laminates with a stacking sequence of [0°/90°] with 4 plies, were manufactured through the hot-pressing technique. The composite laminate was characterized by a fiber volume fraction of about 50% in CF/PPS.

The experimental campaign involved treated and untreated aluminum samples. Untreated aluminum samples were slightly cleaned to remove oil, grease, and powder from the surface. Then, these samples were coupled with the CF-PPS. On the other hand, aluminum treated samples were processed by laser texturing before joining. The treatment was performed on the entire overlapping area (22 × 22 mm^2). To this end, 0–90 straight passes with 300 μm of the distance between consecutive passes were used. This led to square texturing on the surface of the aluminum samples. A 30 W fiber laser (YLP-RA30-1–50-20–20 by IPG) with a peak power of 30 kW was used for laser texturing. During the texturing pretreatment, the pulse frequency was set to 30 kHz and the scanning speed was set to 1000 mm/s. Besides, different texturing strategies (mainly differing by the number of repetitions performed on the same path: 10, 15, and 20) were used. This enabled to produce grooves and protrusions with different depths and heights.

2.2. Joining procedure

Friction assisted joining experiments were performed using an instrumented equipment that enabled the measurement of the processing loads (plunging and torque), and temperature during the joining process. A schematic of the clamping setup and the load cells is reported in Fig. 1. The mandrel was mounted on a universal testing machine model 322.121 by MTS. This enabled to control the position and the plunging load during the process. Temperature measurements were performed using an Infrared Camera model E60 by Flir. IR maps were acquired at the highest available frame rate (30 Hz). The camera was positioned at an angle of 65° to the aluminum sheet at almost 300 mm. Before proceeding with the joining experiments, the aluminum surface was covered with a thin layer of graphite. This enabled to increase the surface emissivity to 0.8 [49].

The tool used in the experiments had a cylindrical shape with a diameter of 10 mm, as reported in Fig. 1. The tool was made of K720 high strength steel by Bohler. During the experiments, the aluminum sheet was placed at the tool side, while the CF-PPS was placed under the aluminum sheet. The overlapping area was 22 × 22 mm^2, as shown in Fig. 2.

The tests were conducted under load control. The joining process was subdivided into three phases, namely: plunging, dwell, and tool retraction. Throughout the process, the tool rotated at a prescribed rotational speed,ω. The process started by plunging the tool towards the aluminum surface (plunging phase) with a prescribed plunging rate P_{rate} until the plunging load P_{max} was reached. Then, the dwell phase started and proceeded for the given dwell time D_t. The plunging load was maintained constant throughout the dwell phase. Finally, the tool was immediately retracted enabling a fast cooling of the sheets. The main process parameters involved in the study are summarized in Table 2. The table also reports the maximum and minimum values used for each process parameter. These values were selected based on previous experiences of laser texturing and friction assisted joining, as well as preliminary experiments and equipment limits.

2.3. Quality assessment

The mechanical behavior of the joints was assumed as the key quality parameter of the joints. To this end, single-lap shear tests were conducted under quasi-static conditions (at a traverse speed of 1 mm/min). A schematic of the sample used in mechanical characterization

Table 1
Main characteristics of involved materials.

	Young's Modulus [GPa]	Yield Strength [MPa]	Tensile Strength [MPa]	Melting temperature [°C]	Glass Transition Temperature [°C]
AA7075	72	575	530	620	–
PPS	3.5	87	90	280	90

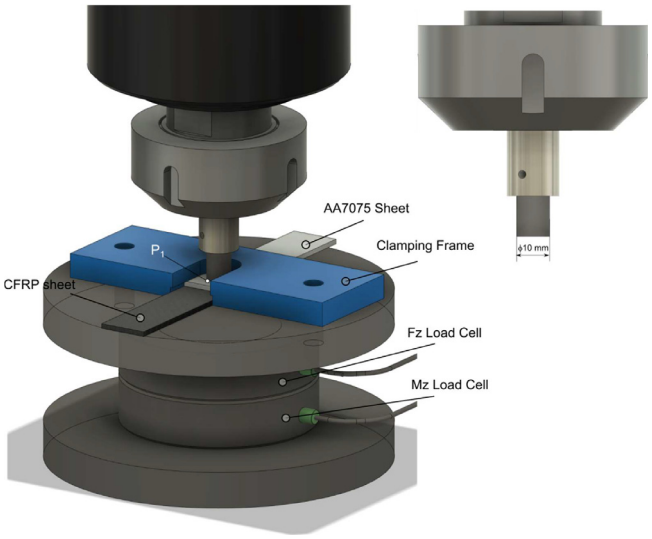

Fig. 1. (a) Schematic of the friction-assisted joining equipment and (b) detailed view of the tool.

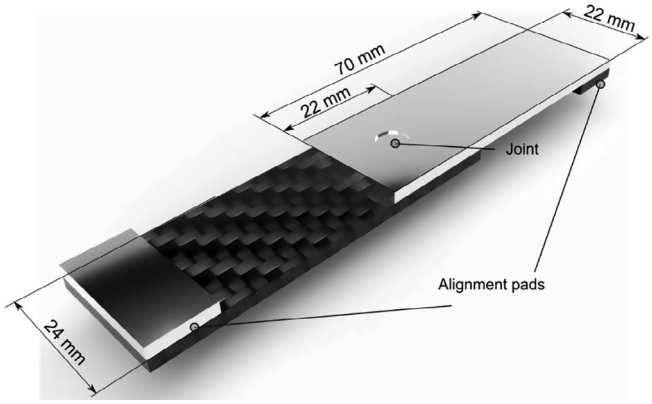

Fig. 2. Schematic of the specimen used in single-lap shear tests.

tests is reported in Fig. 2. A universal testing machine model C43.504 by MTS equipped with a load cell with a 50 kN full scale was adopted. For each testing condition, at least five replicates were performed. Then, the mean and standard deviation values were calculated. Fracture surface analysis was conducted on the samples after the tensile tests. To this end, a stereoscope model M205 by Leica was adopted. The adoption of a motorized 3D table embedded into the stereoscope along with the software LEICA MAP enabled the 3D reconstruction of the fractured surfaces. Also, to better understand the material flow and the joining mechanism, cross-sections of joined samples were analyzed. Standard metallographic procedures were followed to prepare the samples for the optical analysis. These cross-sections were observed using a metallographic microscope model DMI5000M by Leica.

3. Results

Fig. 3a depicts the 3D surface topography of an aluminum sample treated with 20 repetitions. The virtual cross-section depicted in Fig. 3c indicates that the teeth were 35 ± 5 μm tall. The same analysis was performed to characterize the texture produced with a different number of repetitions. The height of the teeth increased almost linearly with the number of repetitions, as depicted in Fig. 3b.

3.1. Mechanism of bonding

The shear tests performed on joints made by untreated aluminum samples indicated a poor adhesion of the substrates (the ultimate shear force reached up to 120 N). These results were in disagreement with those reported by Amancio et al. [26] concerning the friction spot joining process. This difference was addressed to the higher pressure involved in friction spot joining that enabled mechanical fastening between the aluminum and glass or carbon fibers as well as the microinterlocking of the natural asperities on the aluminum surface with the underlying component. On the other hand, the joints made by the texturized aluminum samples showed a higher strength. Before analyzing the influence of the process parameters on the quality of the joints, the main features of a reference joint are examined. Fig. 4 shows the fracture surface of the CF-PPS laminate of a joint produced with $\omega = 8000$ RPM, $P_{max} = 1000$ N, $S_p = 100$ N/s, and $D_t = 4$ s (overall joining time: 14 s). The aluminum sample was texturized with 20 repetitions.

The morphology in Fig. 4 reveals the typical features of the joint. The central region of the joint (in correspondence with the tool) shows a depression area with a great loss of thermoplastic matrix. The PPS was ejected from the central region and was pushed towards the surrounding areas owing to the higher temperatures and pressure. Besides, the prolonged action of the tool (under this condition the overall interaction time was 14 s) produced a progressive compression action that deformed the aluminum sheet as well as the underlying CFRP laminate. The PPS matrix flowed from the depression area towards the peripherical regions (characterized by lower pressure and temperature). The entire metal-composite overlapping area was characterized by the indentations released by the aluminum texture protrusions on the CFRP surface. The indentations were deeper in the central region as compared to the periphery as the difference in the temperature and pressure distribution. A large amount of PPS was ejected from the intersection of the carbon fibers weft and warp, where a higher amount of polymer was present. This can be better

Table 2
Range of joining parameters.

Levels	Tool rotation speed, ω [RPM]	Plunging rate, P_{rate} [N/s]	Plunging Load, P_{max} [N]	Dwell Time, D_t [s]	Number of passes of laser texturing
Minimum	6000	100	300	0	0 – not texturized
Maximum	8000	1000	1000	15	20 – texturized

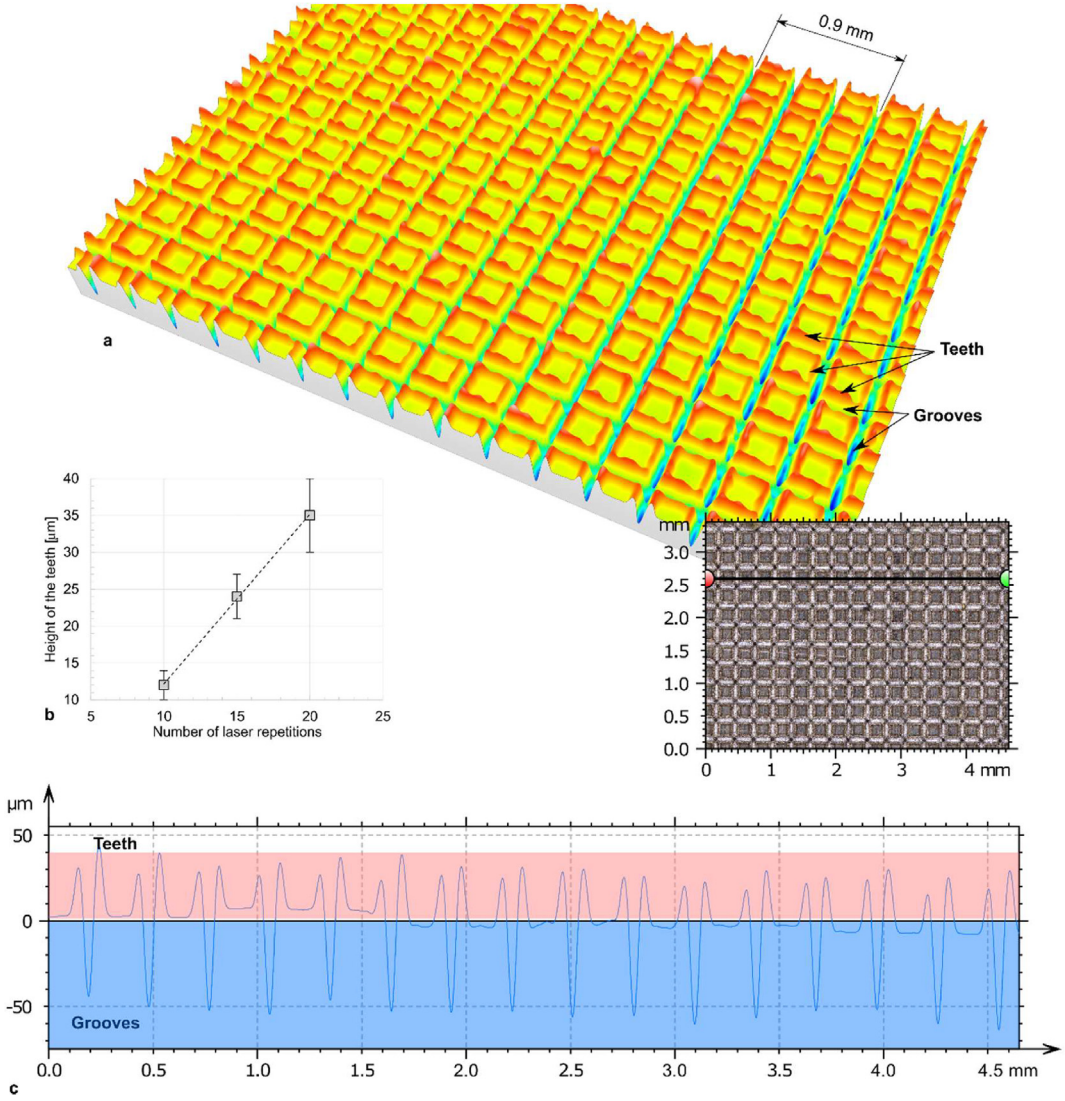

Fig. 3. (a) 3D topography of the aluminum surface after laser texturing was performed with 20 repetitions; (b) virtual cross-section performed on the surface.

appreciated in Fig. 5, which shows the loss of (PPS) material in the region surrounding the depression area (Fig. 5c and d).

The upper layer of the central region was almost completely deprived of the polymeric matrix, as shown in Fig. 6. Here, a closer observation of the CF-PPS surface reveals the formation of a pattern of carbon fibers. These fibers were aligned along the grooves produced on the aluminum surface. Besides, in some limited regions, some square areas with patterns of Carbon fibers perpendicular to the main direction can be observed. This spatial arrangement reflects the weft and warp distribution of the top CF-PPS layer, as shown in Fig. 6c and d. For easier identification of the correspondences, the horizontal areas were colored and labeled from A1 to A5.

The aluminum substrate, depicted in Fig. 7, shows the presence of carbon fibers "trapped" within the grooves of the texture made on the aluminum surface. These fibers were all aligned transverse to the loading direction. This would suggest a possible contribution to the load-bearing capacity of the joint. Besides, the higher magnification macrograph shown in Fig. 7b indicates the presence of a great amount of PPS attached to the aluminum texture.

Further investigation was performed to deeply understand the mechanism of bonding. Fig. 8a depicts the cross-section of a sample made under the same processing conditions.

The aluminum teeth slightly indented the first layer of carbon fibers. This was due to the high stiffness of the CFRP laminate and relatively low pressure exerted by the tool on the aluminum sheet. The joint cross-section is characterized by different regions. In the central region, the PPS matrix tended to fulfill the grooves realized on the aluminum surface (solidified PPS), as depicted in Fig. 8c. Similarly, the carbon fibers aligned along the texture grooves showed higher "flowability" and tended to move towards these grooves. This was facilitated by the high temperature reached (on the top aluminum surface the peak temperature was almost 420 °C) by the PPS matrix. This led to lower polymer viscosity and consequently greater mobility of the fibers. In peripherical regions, where higher temperatures were expected (as the higher tangential speed), the metal-composite interface was characterized by the presence of porosities, as shown in Fig. 8c. These were due to different causes including moisture trapped within the composite, as well as the air trapped at the aluminum and the CFRP interface. The presence of these porosities affected the quality of the joints as they acted as a stress raiser and reduced the contact surface between the substrates. During the joining process (conducted at ω = 8000 RPM, P_{max} = 1000 N, S_p = 100 N/s, and D_t = 4 s), the aluminum temperature exceeded 420 °C. This involved a severe flow stress reduction and consequently, even low plunging force-induced severe plastic deformation on the aluminum sheet. This finally resulted

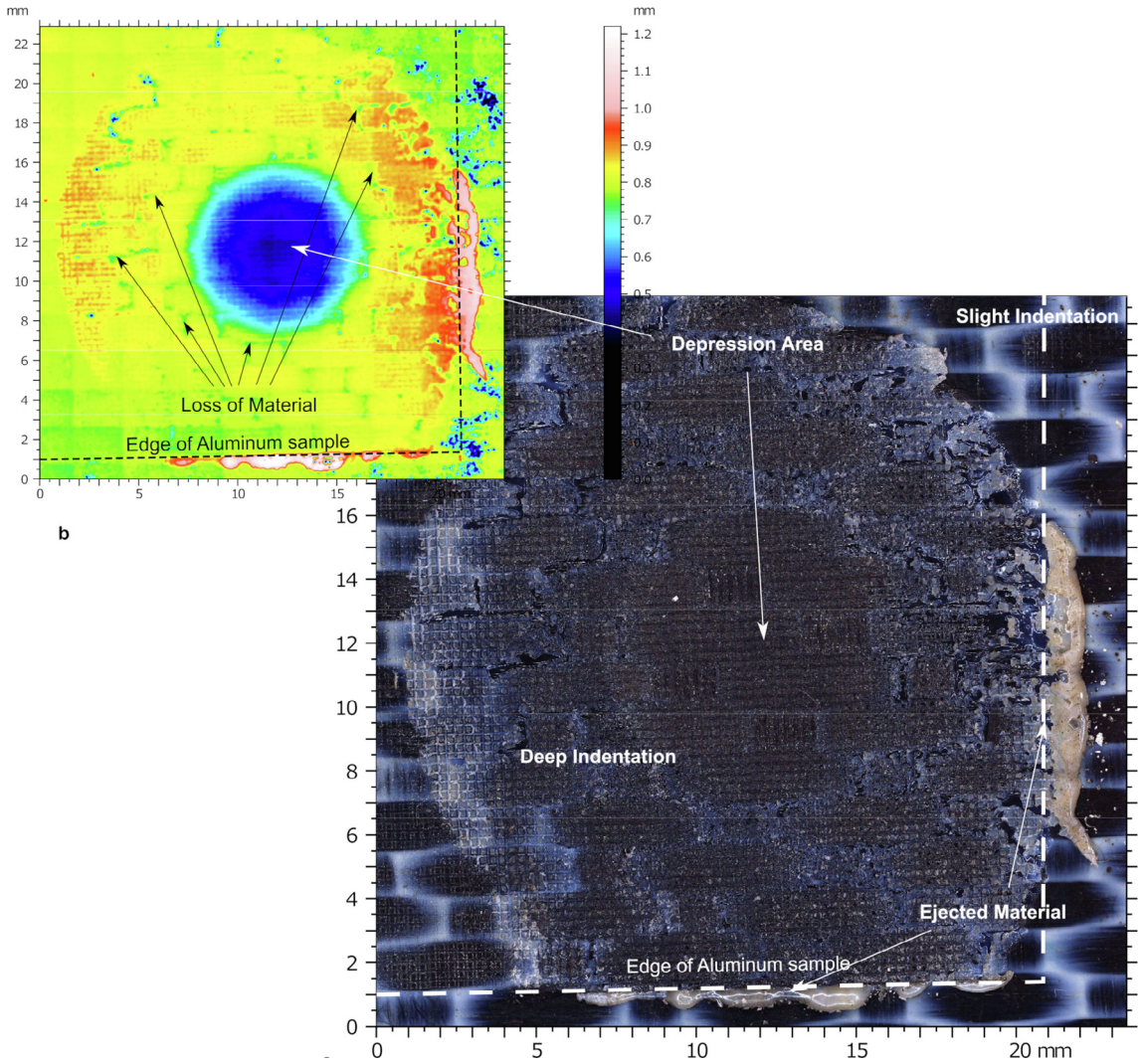

Fig. 4. Fractured PPS-CF/AA7075 joint – CFRP Substate. Processing conditions: ω = 8000 RPM, P_{max} = 1000 N, S_p = 100 N/s and D_t = 4 s.

in a concave bottom surface development. Besides, the underlying composite showed uneven stiffness distribution as the melting temperature of the polymeric matrix was exceeded. Thus, in the central region (in correspondence with the tool area), the aluminum tended to draw with consequent formation of the abovementioned depression area. Surrounding regions, which were characterized by lower temperatures, were more prone to deform elastically. This involved a change in the curvature of the contact region. During the cooling phase, differential shrinking developed, and the aluminum sheet exhibited counter bending. This triggered the separation of the substrates, as shown in Fig. 8b, even though the clamping frame was involved during all cooling/consolidation phase.

3.2. Effect of process parameters

Based on the above-mentioned observations, the joining mechanism, the strength, and the presence of defects depended on several aspects, including:

- the viscosity/temperature of the PPS matrix of the CFRP laminate that may hinder the fulfillment of the interfacial gaps;
- the pressure applied by the aluminum teeth on the underlying carbon fibers;
- the height of the aluminum teeth and the depth of the grooves;
- the relative orientation of the laminate to the loading direction;

In the following section, these processing factors were analyzed by varying the main process parameters.

3.2.1. Effect of the plunging load and dwell time

The variation of the peak temperature measured over the aluminum surface during the joining process is reported in Fig. 9 for different values of the plunging load P_{max} and holding fixed the tool rotation speed (ω = 8000 RPM) and the Dwell time (D_t = 15 s). The curves reported the temperature at a point P_1 (shown in Fig. 1), which was analyzed frame by frame. The length of the plunging phase depended on P_{max} (the plunging phase lasted P_{max}/P_{rate}). Therefore, the plunging phase ranged between 0.3 s and 0.8 s (for P_{max} = 300 N and 800 N, respectively).

When the process began, the temperature trends showed a steep increase; then, the curve slope decreased, and saturation prevailed. This was due to two different phenomena. Higher plunging loads involved fast heating and higher processing temperatures as higher frictional heat was produced. However, the temperature saturated at 420–430 °C. At this temperature, the aluminum was highly softened (almost pasty) and higher plunging loads determined a larger amount of aluminum reflow rather than higher temperature. Tests conducted with P_{max} = 1000 N led to severe thinning of the aluminum sheet in

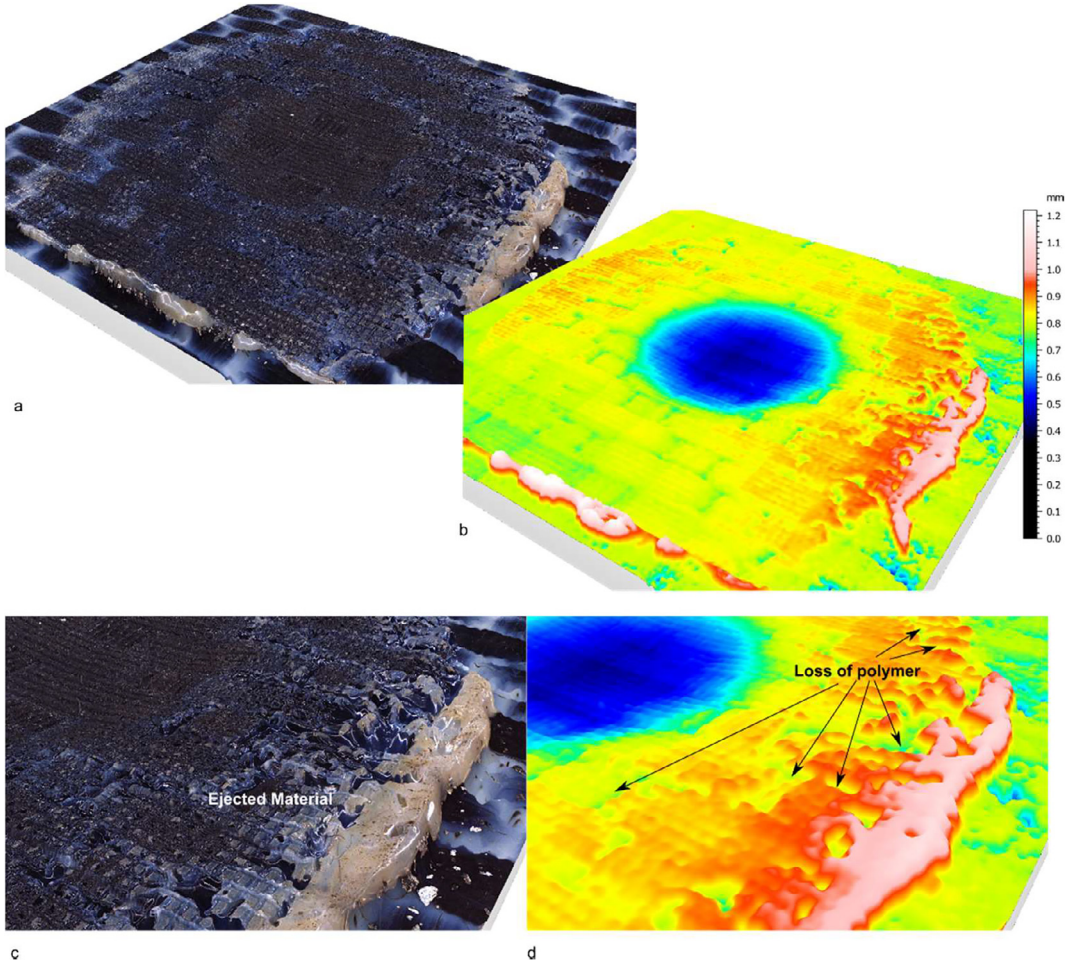

Fig. 5. (a, c) Morphology and (b, d) 3D reconstruction topography of CFRP fracture surface showing ejected material and loss of polymer. Processing conditions: ω = 8000 RPM, P_{max} = 1000 N, S_p = 100 N/s and D_t = 4 s.

correspondence of the contact area with the punch, as shown in Fig. 10. On the other hand, when low plunging loads were adopted (e.g., P_{max} = 300 N and 400 N), heat diffusion effects prevailed, leading to a limited temperature increase even after long dwell times. This was due to the heat loss towards the clamping system, the radiation, and the convection, as discussed in [50]. At the end of the process, the temperature steeply reduced (up to 40 °C/s), leading to a fast joint consolidation., the temperature decreased very quickly, and the joint consolidated.

The influence of the plunging load on the peak temperature of texturized and untreated samples is reported in Fig. 11. These tests were performed with ω = 8000 RPM and D_t = 15 s. Texturized samples were characterized by higher temperatures than untreated ones, at equal plunging load. This was due to the smaller contact interface that limited the heat diffusion from the aluminum to the CF-PPS surface. This caused higher temperatures experienced by the aluminum sheet. Both the trends concerning texturized and untreated samples were characterized by saturation (plateau) as the temperature exceeded 410–430 °C.

It must be concerned that, the temperatures depicted in Figs. 9 and 11 refer to the peak temperature measured over the aluminum sample; therefore, they are higher than the temperature at the metal-composite interface. The experimental measurement of the temperature at the interface is very complex. However, according to the results reported in [51], where the same aluminum alloy was employed and similar processing conditions were adopted, the temperature at the metal-composite interfaces should be 30–40 °C lower than that observed at the upper metal surface.

Fig. 12a depicts the influence of the plunging load and dwell time on the ultimate shear force (F_r). The minimum plunging load required to join the substrates was 400 N. Indeed, as reported in Fig. 11, a plunging load of 300 N involved a processing temperature of almost 200 °C, which was much lower than the melting temperature of the PPS (280 °C). Higher plunging loads involved higher F_r values (up to 10.7 kN). Fig. 12b indicates that the increase of F_r with the plunging load was due to the achievement of higher temperatures. All the F_r values fit a second-order polynomial, regardless of the plunging load and the dwell time.

Fig. 12c-f show the macrographs of the CF-PPS substrates of some samples joined under different conditions. The comparison among the macrographs indicates that the increase of the USF was determined by the increase of the joining area. The CF-PPS substrate produced under different processing temperatures were characterized by different morphologies. Under relatively low temperatures, the bonding area is partially covered by the PPS matrix ejected from the laminate. Higher processing temperatures produced lower PPS viscosity. This led to a higher amount of PPS ejected from the laminate with a severe impoverishment of PPS especially in correspondence of the intersection between the weft and the warp. This can be better observed in Fig. 13. Here, the 3D reconstruction of the fracture surface highlights the presence of regions where the ejected PPS matrix tended to accumulate (mainly at the periphery of the joined area). Besides, Fig. 13b and d show that the PPS matrix was also ejected from the carbon fiber

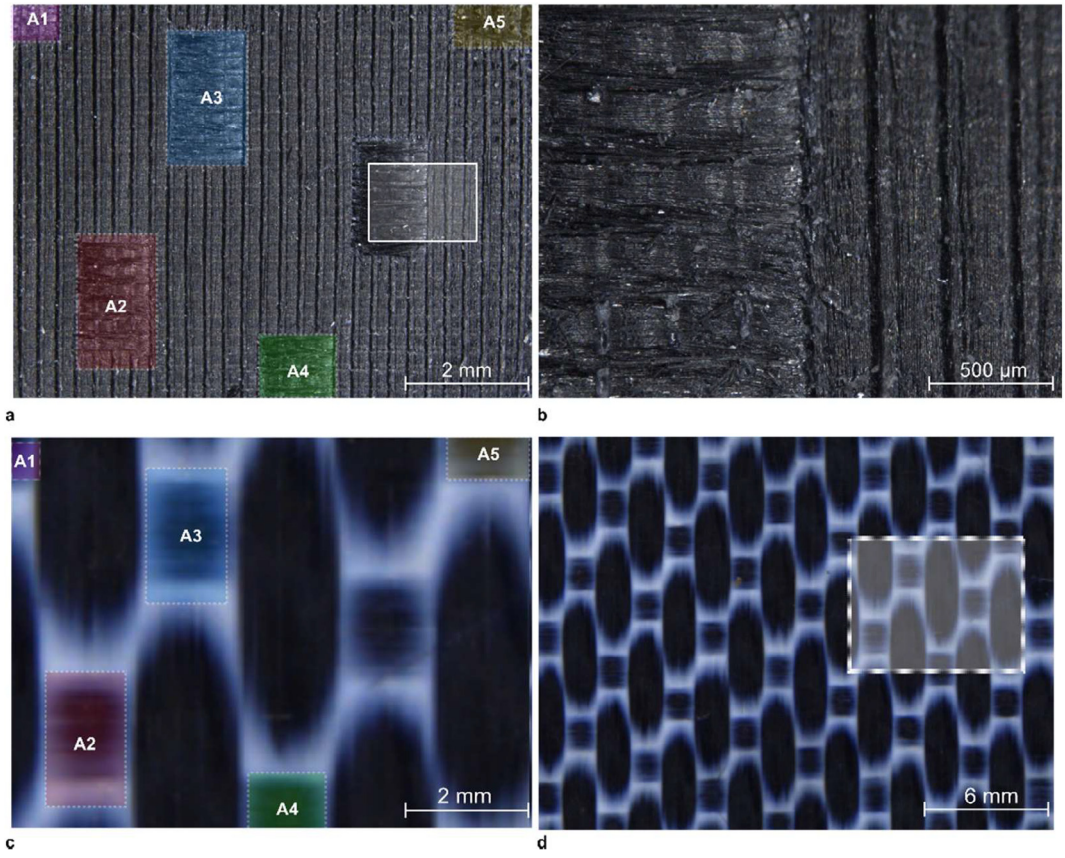

Fig. 6. (a-b) Macrographs of the central region of CFRP fracture surface showing the absence of polymer, performed at (a) low and (b) higher magnifications. (Processing conditions: ω = 8000 RPM, P_{max} = 1000 N, S_p = 100 N/s and D_t = 4 s); (c) high and (d) low magnification of weft and warp disposition on CF-PPS.

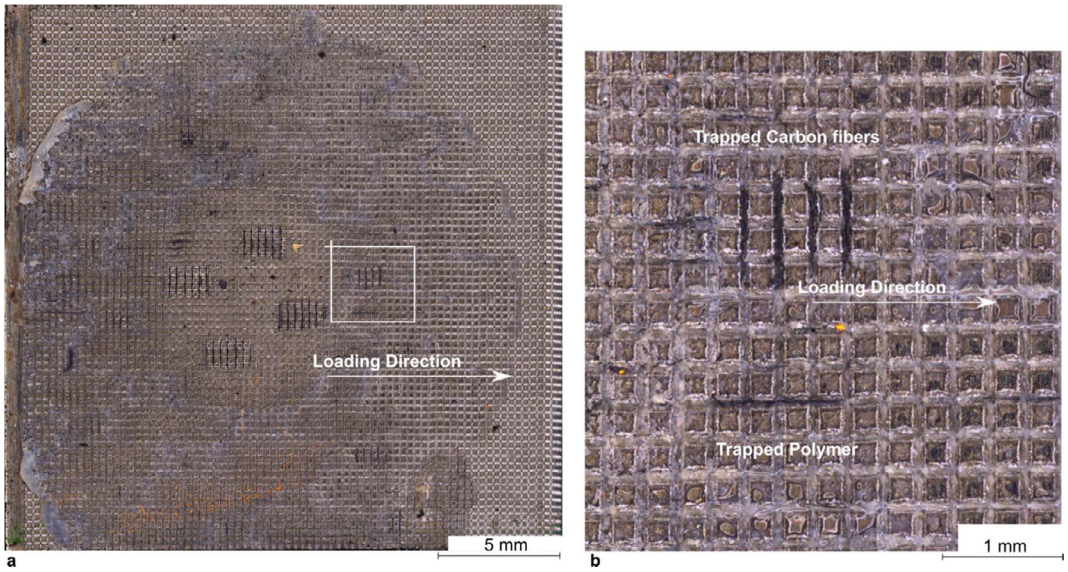

Fig. 7. Fractured PPS-CF/AA7075 joint – Aluminum substate, performed at (a) lower and (b) higher magnifications. Processing conditions: ω = 8000 RPM, P_{max} = 1000 N, S_p = 100 N/s and D_t = 4 s.

bundles. Fig. 13d depicts the presence of a pattern disposition of PPS that arranges along the texture grooves (produced on the aluminum surface).

3.2.2. *Influence of the texture and loading direction*

Fig. 14 shows the influence of the texturing characteristics made on the aluminum surface and the contribution of the carbon fibers to the

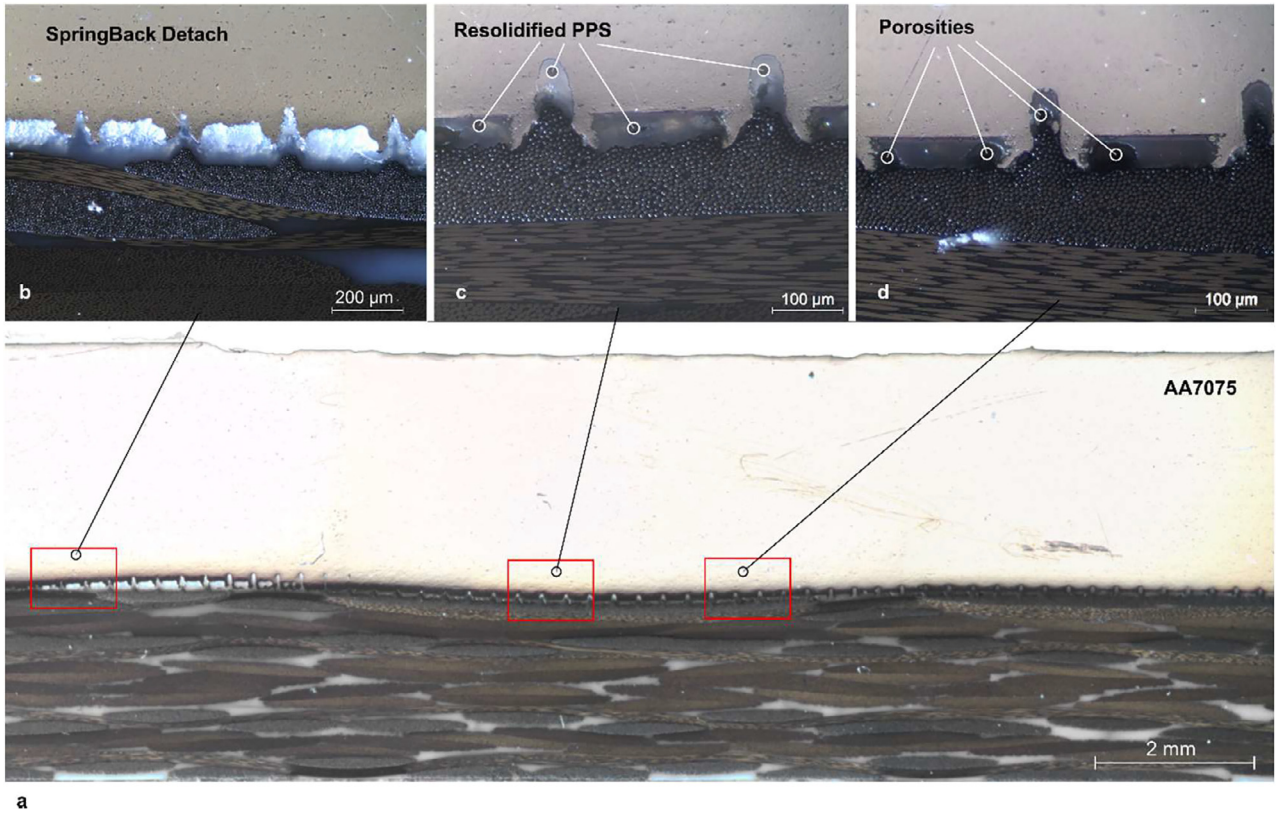

Fig. 8. (a) Cross-section of the joint showing different characteristic regions (b) Springback detach; (c) fulfilled interface and (d) presence of porosities.

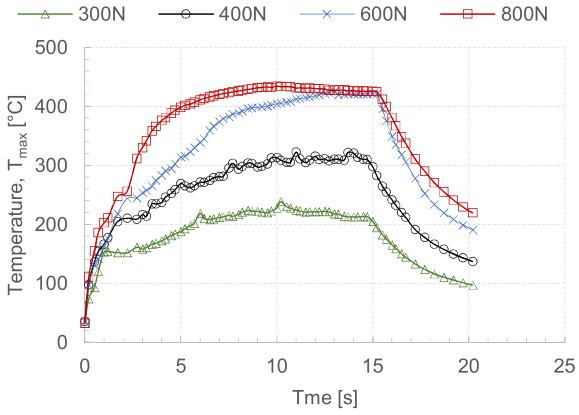

Fig. 9. Variation of the temperature at the tool edge with time for different levels of plunging loads (ω = 8000 RPM, P_{rate} = 1000 N/s, Dt = 15 s).

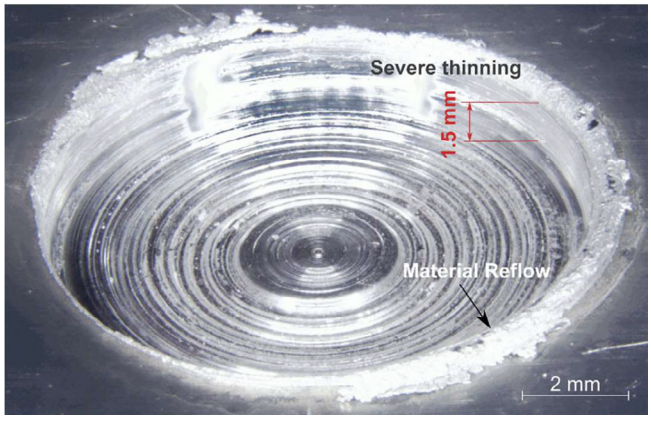

Fig. 10. Macrograph of the upper surface of a specimen processed with excessively high plunging force (P_{max} = 1000 N), ω = 8000 RPM, and D_t = 15 s.

ultimate shear force. The adoption of a texture with taller teeth and deeper grooves (using a higher number of texturing passes) produced joints with higher strength. The increase in the number of passes from 10 to 20 passes enabled to increase the shear force by almost 20%. On the other hand, the comparison between the tests conducted transverse and parallel to the fiber direction indicates a moderate contribution of the fibers to the strength of the joints (almost 10%).

3.2.3. Reducing the indentation on the aluminum surface

Additional tests were performed to avoid the severe deformation of the aluminum and the consequent depression area released on the CFRP upper surface. To this end, the tests were performed by using a lower plunging load (P_{max} = 500 N) and varying the dwell time between 5 and 15 s. The adoption of a reduced plunging load enabled to avoid the high deformation on the aluminum. This produced a lower pressure (exerted by the tool on the metal sheet) and a lower temperature reached during the process. Fig. 15 indicates that even with the longer dwell time (Dt = 15 s), the temperature did not exceed 340 °C. Thus, even though a lower frictional power was produced, the adoption of moderate pressures can eliminate the onset of severe deformation of the upper aluminum surface as well as the depression area on the CFRP laminate.

The fracture surfaces reported in Fig. 15 confirms the above trends. Indeed, the ultimate shear force increased with the dwell time as higher temperatures were reached. This came with larger joined areas and consequently higher ultimate shear force.

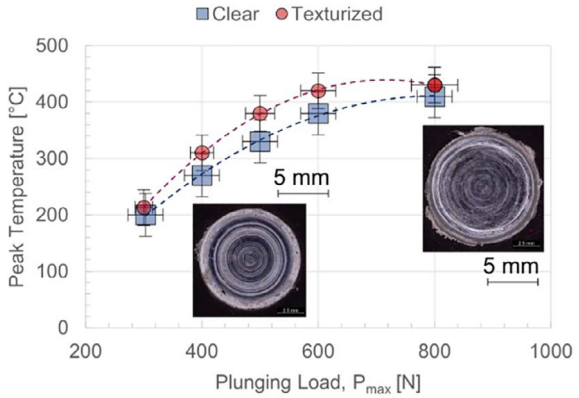

Fig. 11. Variation of the peak temperature with the plunging load (ω = 8000 RPM, P_{rate} = 1000 N/s, D_t = 15 s).

4. Discussion

Hybrid Structures (HS) made by lightweight materials such as aluminum alloys and Carbon Fiber reinforced plastic represent a great opportunity for the transportation industry as well as the biomedical sector because HSs enable higher performances and high design flexibility. The growing spreading of Carbon Fiber reinforced thermoplastics is driven by demands of reuse, reutilize, and recycle that constitute the fundaments of the circular economy. The possibility of "material reshaping" enables the possibility of using new joining processes based on material deformation to produce mechanical joining between dissimilar materials. So far, Friction Assisted Joining has been successfully employed to join metals with thermoplastics; however, FAJ has not yet tested for joining metals with reinforced thermoplastics. Here, the presence of dense bundles of fibers may hinder the material flow during the joining process.

This study investigated for the first time the possibility to adopt the Friction Assisted Joining process to join aluminum alloy (AA7075) and CF-PPS through an experimental approach. The results indicated that the process is characterized by a temperature threshold that triggers substrates bonding. The matrix material flows towards the asperities produced on the aluminum surface leading to the formation of micro interlocking that mechanically fastens the substrates. This also pushes the carbon fibers to flow towards the grooves produced on the aluminum surface (by laser texturing). However, the contribution of the fibers was limited to a moderate extent (almost 10%). The results indicated that the bonding mechanism was still based on mechanical fastening between the aluminum and the polymer; however, the material flow was different from that observed in FAJ of metals with thermoplastics. Indeed, the high stiffness of the CF-PPS hindered the deep penetration of the aluminum teeth within the carbon fibers. Therefore, the high pressure exerted by the aluminum teeth on the composite surface and temperature at the interface led to polymer reflow towards the interstices of the aluminum surface. The results indicated that the bonding mechanism was mainly temperature-dependent. Indeed, when the temperature exceeded 260 °C the substrates were joined. The Ultimate Shear force increased with the processing temperature. This was mainly due to a larger extension of the region exceeding the threshold temperature. However, because of the difference in temperature distribution, as well as pressure distribution, the joints showed uneven morphologies.

The mechanism of bonding was mainly due to the PPS matrix-metal texture interaction, while the fibers showed a minor contribution to the load-bearing capability of the joints (almost 10%). Similarly, the depth of the teeth (produced with different laser scanning repetitions) improved the strength of the joints, but the increase in USF was only 10–20%. The slight penetration of the aluminum teeth through the carbon fibers was due to the interweaving warp weft of the fibers. This

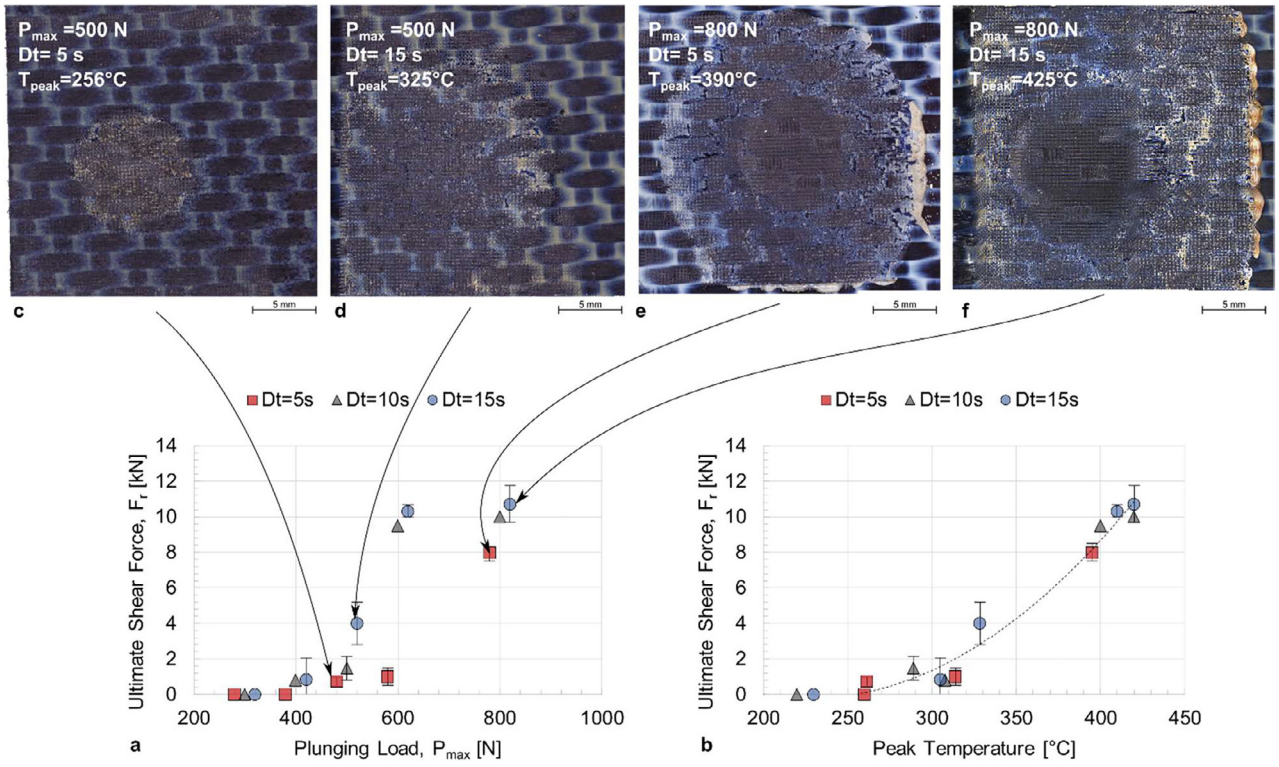

Fig. 12. (a) Influence of plunging load and dwell time and (b) peak temperature on the ultimate shear force. Macrographs of CFRP substrate after testing showing the increase of the joining area with processing temperature.

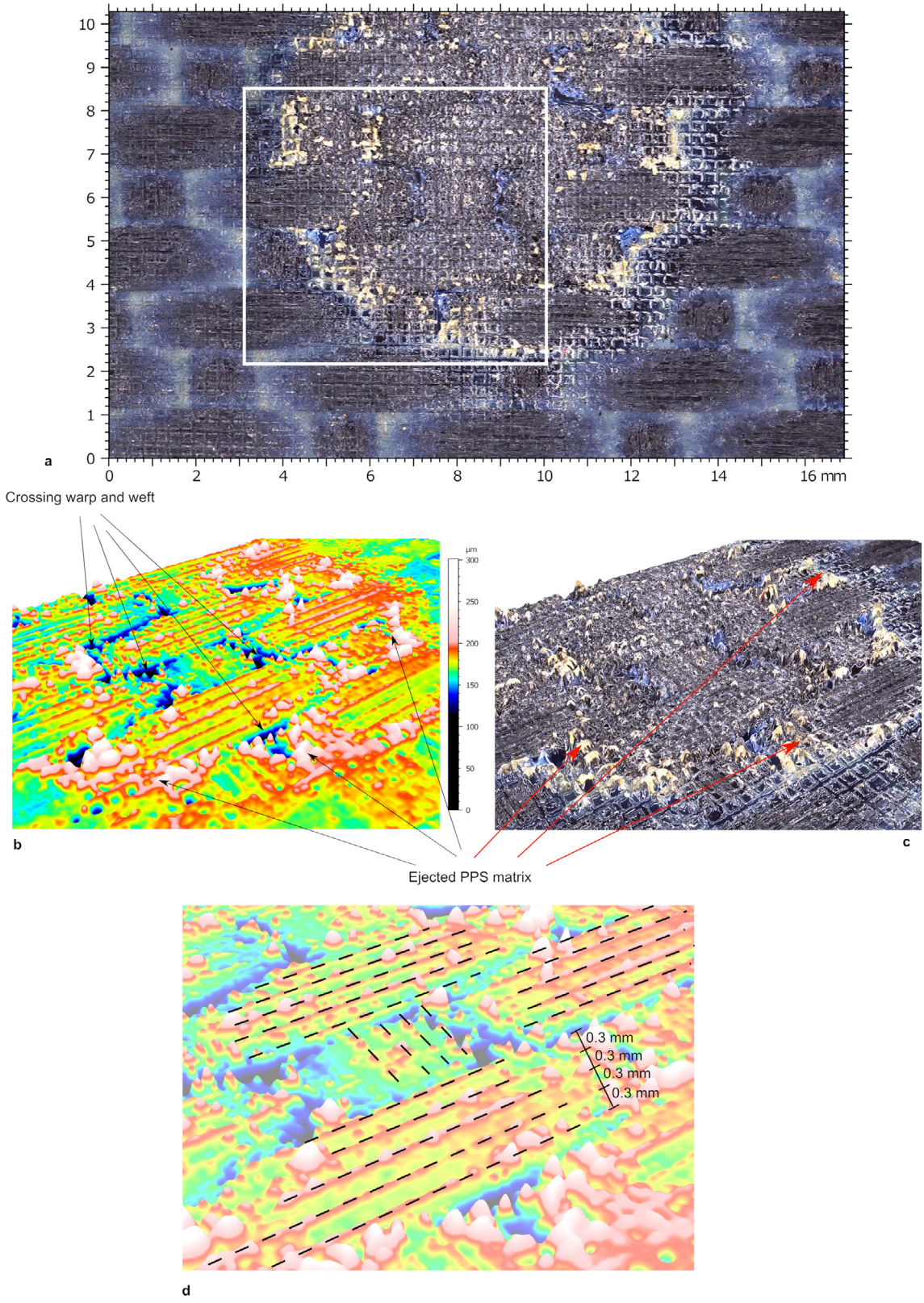

Fig. 13. Macrographs of CFRP substrate showing the PPS matrix ejection. (a) Fracture surface; (b) false-color topological reconstruction; (c) true color topological reconstruction and (d) pattern of ejected PPS formed along the aluminum grooves.

greatly inhibited the flow of fibers within the grooves produced on the aluminum surface. Indeed, only a small amount of carbon fibers tended to flow within the texture grooves produced on the aluminum surface. Deeper grooves (achieved by increasing the number of laser scans during the metal surface texturing) did not provide significant improvements in terms of mechanical behavior.

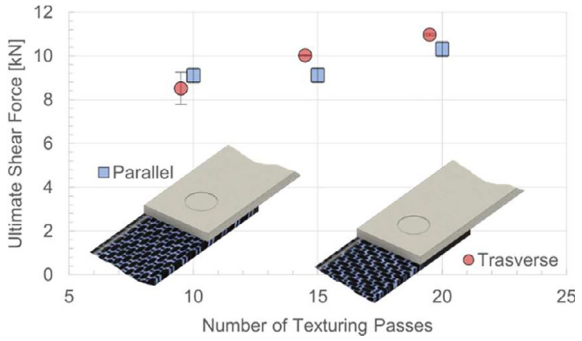

Fig. 14. Effect of fibers orientation and texturing strategy.

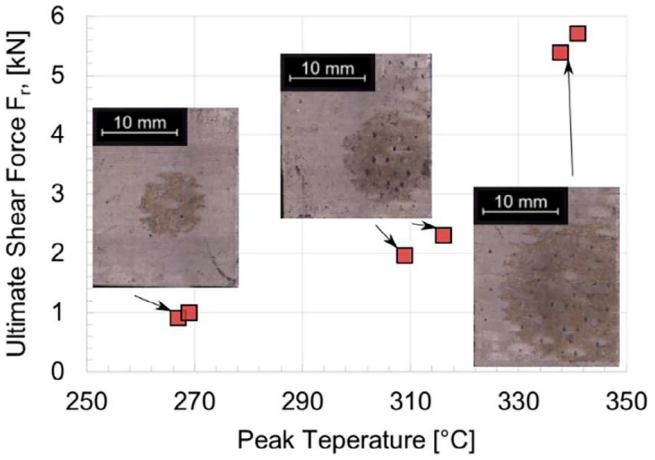

Fig. 15. Variation of the ultimate shear force with peak temperature and aluminum fracture surfaces for samples joined with a plunging load of 500 N.

Even though a direct comparison with other processes is often difficult owing to a difference in materials, material preparation, and even testing procedures, a qualitative comparison of the shear strength of the joints produced through FAJ and other joining processes is presented in Fig. 16. The strength of the joints is comparable and often higher than other competitive processes (i.e. injection molding, adhesive bonding, and induction welding). The joints made by FAJ showed similar strength to those produced by friction stir riveting, friction stir welding, laser-assisted joining; however, friction spot joining, and ultrasonic welding provided higher strengths. It must be noted that both ultrasonic welding and friction spot joining processes have a greater maturity since they were developed almost ten years ago. This enabled us to explore possible improvements (such as the adoption of a polymer interlayer [52,53] between the adherends). The shear strength of the joints made in this work is also compared to that achieved in previous studies concerning unreinforced plastics. When used to join metals to unreinforced thermoplastic, FAJ enabled higher strength (please note that in the case of AA5053/PVC joints the joint efficiency reached almost 98%). This seems to indicate that the carbon fibers exerted a detrimental effect on the joining strength as they inhibited the mutual interlocking between the aluminum teeth and the PPS matrix. To this end, future studies are demanded to design a more suitable texture, which could accommodate more easily the carbon fiber bundles.

However, the results of this study are extremely encouraging if compared to adhesive bonding. FAJ enabled different advantages, such as a high ultimate shear force, an extremely short joining time (1–3 s for joint), the absence of external hazardous materials (and their storage), no need for surface pretreatment, the easy process automatization, and no need for curing (only relatively short cooling of 5–10 s is needed).

5. Conclusions

A campaign of experimental tests was conducted to determine the suitability of Friction Assisted joining to join Aluminum alloy AA7075 with Carbon Fiber Reinforced PolyPhenylene Sulfide (CF-PPS). The key parameters influencing the strength of the joints were investigated by varying the main process parameters, including the plunging load, dwell time, and texturing strategy. Also, the orientation of the external load to the fibers of the interfacial layer was studied. The main results are reported as follows:

- the process is triggered by the temperature achieved at the metal-composite interface. The threshold temperature was 260 °C. The adoption of processing conditions involving higher temperatures came with higher ultimate shear force (USF). This was due to the increase of the region exceeding the threshold temperature.

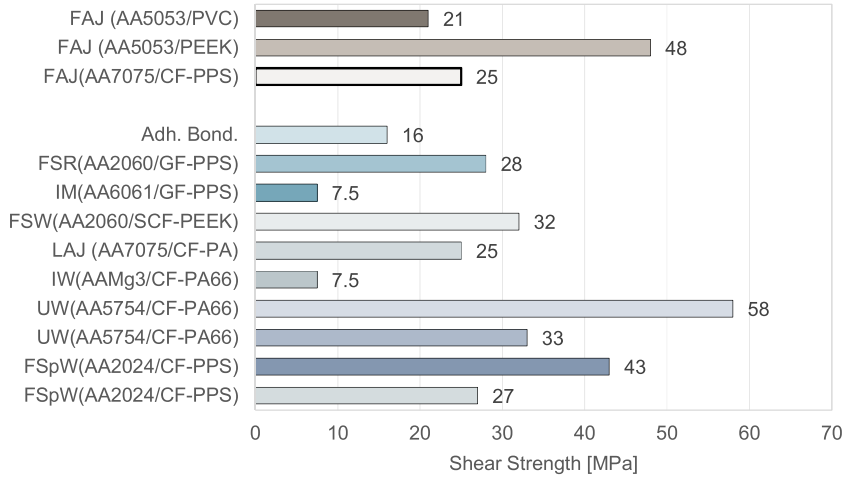

Fig. 16. Comparison of shear strength of different processes used for hybrid joints. FAJ (AA5053/PVC) [50]; FAJ (AA5053/PEEK) [46]; Friction stir Riveting (FSR) [6]; Injection Molding (IM) [8]; Friction Stir welding (FSW) [5]; Laser Assisted Joining (LAJ) [54]; Induction Welding [55]; Ultrasonic Welding (UW) [56]; Friction Spot Joining [23].

- the joining mechanism was based on the mechanical interlocking between the composite matrix (PPS) and the teeth produced on the aluminum surface by laser texturing. The contribution of the carbon fibers to the ultimate shear force was almost 10%;
- the morphology of the fractured surfaces as well as the cross-section of the joints showed different regions. The substrates were characterized by a gap at the side edge of the tool. On the other hand, in the central region, the gaps were filled with a composite matrix. Porosities were observed were higher temperature was reached;
- the presence of the carbon bundles in weft and warp arrangement hindered the mechanism of interlocking between the aluminum texture and PPS matrix. Thus, FAJ of metal to composite laminates requires specific texture designs to limit such an adverse phenomenon.
- the adoption of a plunging load of 800 N enabled to increase the frictional heat produced per unit time. This enabled us to achieve a maximum ultimate shear force up to 10.7 kN with a joining time of 5 s. Further increase of the plunging load, produced severe perforation of the aluminum sheet;

CRediT authorship contribution statement

Francesco Lambiase: Conceptualization, Data curation, Formal analysis, Funding acquisition, Investigation, Methodology, Project administration, Resources, Software, Supervision, Validation, Visualization, Writing - original draft, Writing - review & editing. **Alfonso Paoletti:** Conceptualization, Data curation, Formal analysis, Funding acquisition, Investigation, Methodology, Project administration, Resources, Software, Supervision, Validation, Visualization, Writing - original draft, Writing - review & editing. **Massimo Durante:** Conceptualization, Data curation, Formal analysis, Funding acquisition, Investigation, Methodology, Project administration, Resources, Software, Supervision, Validation, Visualization, Writing - original draft, Writing - review & editing.

Declaration of Competing Interest

The authors declare that they have no known competing financial interests or personal relationships that could have appeared to influence the work reported in this paper.

6. Data Availability

The raw/processed data required to reproduce these findings cannot be shared at this time as the data also forms part of an ongoing study.

Acknowledgments

The authors would like to thank Mr. G. Organtini (DIIIE, University of L'Aquila) for his contribution during the setup and performance of the experimental tests. The authors would also like to acknowledge eng. S. Genna from CIRTIBS for his contribution during material preparation.

References

[1] Kweon J-H, Jung J-W, Kim T-H, Choi J-H, Kim D-H. Failure of carbon composite-to-aluminum joints with combined mechanical fastening and adhesive bonding. Compos Struct 2006;75(1–4):192–8.
[2] Yusof F, Muhamad M, Moshwan R, Jamaludin M, Miyashita Y. Effect of surface states on joining mechanisms and mechanical properties of aluminum alloy (A5052) and polyethylene terephthalate (PET) by dissimilar friction spot welding. Metals 2016;6 (5):101.
[3] Huang Y, Meng X, Xie Y, Wan L, Lv Z, Cao J, Feng J. Friction stir welding/processing of polymers and polymer matrix composites. Compos A Appl Sci Manuf 2018;105:235–57.
[4] Huang Y, Meng X, Xie Y, Li J, Si X, Fan Q. Improving mechanical properties of composite/metal friction stir lap welding joints via a taper-screwed pin with triple facets. J Mater Process Technol 2019;268:80–6.
[5] Huang Y, Meng X, Xie Y, Li J, Wan L. Joining of carbon fiber reinforced thermoplastic and metal via friction stir welding with co-controlling shape and performance. Compos A Appl Sci Manuf 2018;112:328–36.
[6] Meng X, Huang Y, Xie Y, Li J, Guan M, Wan L, Dong Z, Cao J. Friction self-riveting welding between polymer matrix composites and metals. Compos A Appl Sci Manuf 2019;127:105624.
[7] Huang Y, Meng X, Xie Y, Li J, Wan L. New technique of friction-based filling stacking joining for metal and polymer. Compos B Eng 2019;163:217–23.
[8] Li X, Xu D, Gong N, Xu Z, Wang L, Dong W. Improving the strength of injection molded aluminum/polyphenylene sulfide lap joints dependence on surface microstructure and composition. Mater Des 2019;179:107875.
[9] Li X, Liu F, Gong N, Yang C, Wang B. Surface topography induced high injection joining strength of polymer-metal composite and fracture mechanism. Compos Struct 2018;184:545–53.
[10] Blaga L, Bancilă R, dos Santos JF, Amancio-Filho ST. Friction Riveting of glass–fibre-reinforced polyetherimide composite and titanium grade 2 hybrid joints. Mater Des 2013;50:825–9.
[11] Altmeyer J, dos Santos JF, Amancio-Filho ST. Effect of the friction riveting process parameters on the joint formation and performance of Ti alloy/short-fibre reinforced polyether ether ketone joints. Mater Des 2014;60:164–76.
[12] Katayama S, Kawahito Y. Laser direct joining of metal and plastic. Scr Mater 2008;59(12):1247–50.
[13] Yeh R-Y, Hsu R-Q. Development of ultrasonic direct joining of thermoplastic to laser structured metal. Int J Adhes Adhes 2016;65:28–32.
[14] Lionetto F, Balle F, Maffezzoli A. Hybrid ultrasonic spot welding of aluminum to carbon fiber reinforced epoxy composites. J Mater Process Technol 2017;247:289–95.
[15] Lionetto F, Mele C, Leo P, D'Ostuni S, Balle F, Maffezzoli A. Ultrasonic spot welding of carbon fiber reinforced epoxy composites to aluminum: mechanical and electrochemical characterization. Compos B Eng 2018;144:134–42.
[16] Krüger S, Wagner G, Eifler D. Ultrasonic welding of metal/composite joints. Adv Eng Mater 2004;6(3):157–9.
[17] Balle F, Eifler D. Statistical test planning for ultrasonic welding of dissimilar materials using the example of aluminum-carbon fiber reinforced polymers (CFRP) joints. Mat-wiss u Werkstofftech 2012;43(4):286–92.
[18] Wagner G, Balle F, Eifler D. Ultrasonic welding of aluminum alloys to fiber reinforced polymers: ultrasonic welding of Al/FRP-joints. Adv Eng Mater 2013;15 (9):792–803.
[19] Balle F, Huxhold S, Emrich S, Wagner G, Kopnarski M, Eifler D. Influence of heat treatments on the mechanical properties of ultrasonic welded AA 2024/CF-PA66-joints. Adv Eng Mater 2013;15(9):837–45.
[20] Magin J, Balle F. Solid state joining of aluminum, titanium and their hybrids by ultrasonic torsion welding. Materialwiss Werkstofftech 2014;45(12):1072–83.
[21] Staab F, Balle F. Ultrasonic torsion welding of ageing-resistant Al/CFRP joints: Properties, microstructure and joint formation. Ultrasonics 2019;93:139–44.
[22] Junior WS, Handge UA, dos Santos JF, Abetz V, Amancio-Filho ST. Feasibility study of friction spot welding of dissimilar single-lap joint between poly(methyl methacrylate) and poly(methyl methacrylate)-SiO2 nanocomposite. Mater Des 2014;64:246–50.
[23] Goushegir SM, dos Santos JF, Amancio-Filho ST. Friction Spot Joining of aluminum AA2024/carbon-fiber reinforced poly(phenylene sulfide) composite single lap joints: Microstructure and mechanical performance. Mater Des 2014;54:196–206.
[24] Esteves JV, Goushegir SM, dos Santos JF, Canto LB, Hage Jr E, Amancio-Filho ST. Friction spot joining of aluminum AA6181-T4 and carbon fiber-reinforced poly (phenylene sulfide): Effects of process parameters on the microstructure and mechanical strength. Mater Des 2015;66:437–45.
[25] Goushegir SM, dos Santos JF, Amancio-Filho ST. Influence of process parameters on mechanical performance and bonding area of AA2024/carbon-fiber-reinforced poly(phenylene sulfide) friction spot single lap joints. Mater Des 2015;83:431–42.
[26] Amancio-Filho ST, Bueno C, dos Santos JF, Huber N, Hage E. On the feasibility of friction spot joining in magnesium/fiber-reinforced polymer composite hybrid structures. Mater Sci Eng A 2011;528(10-11):3841–8.
[27] Yusof F, Miyashita Y, Seo N, Mutoh Y, Moshwan R. Utilising friction spot joining for dissimilar joint between aluminium alloy (A5052) and polyethylene terephthalate. Sci Technol Weld Joining 2013;17(7):544–9.
[28] Huang Y, Meng X, Xie Y, Lv Z, Wan L, Cao J, Feng J. Friction spot welding of carbon fiber-reinforced polyetherimide laminate. Compos Struct 2018;189:627–34.
[29] Nagatsuka K, Yoshida S, Tsuchiya A, Nakata K. Direct joining of carbon-fiber–reinforced plastic to an aluminum alloy using friction lap joining. Compos B Eng 2015;73:82–8.
[30] Wirth FX, Zaeh MF, Krutzlinger M, Silvanus J. Analysis of the bonding behavior and joining mechanism during friction press joining of aluminum alloys with thermoplastics. Proc CIRP 2014;18:215–20.
[31] Okada T, Uchida S, Nakata K. Direct joining of aluminum alloy and plastic sheets by friction lap processing. Mater Sci Forum 2014;794–796:395–400.
[32] Liu FC, Liao J, Nakata K. Joining of metal to plastic using friction lap welding. Mater Des 2014;54:236–44.
[33] Liu FC, Nakata K, Liao J, Hirota S, Fukui H. Reducing bubbles in friction lap welded joint of magnesium alloy and polyamide. Sci Technol Weld Joining 2014;19(7):578–87.

[34] Derazkola HA, Khodabakhshi F, Simchi A. Friction-stir lap-joining of aluminium-magnesium/poly-methyl-methacrylate hybrid structures: thermo-mechanical modelling and experimental feasibility study. Sci Technol Weld Joining 2018;23 (1):35–49.
[35] Liu FC, Dong P, Lu W, Sun K. On formation of Al O C bonds at aluminum/ polyamide joint interface. Appl Surf Sci 2019;466:202–9.
[36] Rodríguez-Vidal E, Sanz C, Soriano C, Leunda J, Verhaeghe G. Effect of metal micro-structuring on the mechanical behavior of polymer–metal laser T-joints. J Mater Process Technol 2016;229:668–77.
[37] Rodríguez-Vidal E, Sanz C, Lambarri J, Quintana I. Experimental investigation into metal micro-patterning by laser on polymer-metal hybrid joining. Opt Laser Technol 2018;104:73–82.
[38] Jung D-J, Cheon J, Na S-J. Effect of surface pre-oxidation on laser assisted joining of acrylonitrile butadiene styrene (ABS) and zinc-coated steel. Mater Des 2016;99:1–9.
[39] Aliasghari S, Ghorbani M, Skeldon P, Karami H, Movahedi M. Effect of plasma electrolytic oxidation on joining of AA 5052 aluminium alloy to polypropylene using friction stir spot welding. Surf Coat Technol 2017;313:274–81.
[40] Liu H, Jiang Y, Tan W, Wang X. Enhancement of the laser transmission weldability between polyethylene and polyoxymethylene by plasma surface treatment. Materials (Basel) 2017;11 (1).
[41] Zhang Z, Shan J-G, Tan X-H, Zhang J. Effect of anodizing pretreatment on laser joining CFRP to aluminum alloy A6061. Int J Adhes Adhes 2016;70:142–51.
[42] Yusof F, Yukio M, Yoshiharu M, Abdul Shukor MH. Effect of anodizing on pulsed Nd:YAG laser joining of polyethylene terephthalate (PET) and aluminium alloy (A5052). Mater Des 2012;37:410–5.
[43] Lambiase F, Genna S. Experimental analysis of laser assisted joining of Al-Mg aluminium alloy with Polyetheretherketone (PEEK). Int J Adhes Adhes 2018;84:265–74.
[44] Lambiase F, Genna S. Laser assisted joining of AA5053 aluminum alloy with polyvinyl chloride (PVC). Opt Laser Technol 2018;107:80–8.
[45] Lambiase F, Paoletti A. Friction Assisted Joining of titanium and polyetheretherketone (PEEK) sheets. Thin-Walled Struct 2018;130:254–61.
[46] Lambiase F, Paoletti A. Mechanical behavior of AA5053/polyetheretherketone (PEEK) made by Friction Assisted Joining. Compos Struct 2018;189:70–8.
[47] Lambiase F, Grossi V, Paoletti A. Machine learning applied for process design of hybrid metal-polymer joints. J Manuf Process 2020;58:92–100.
[48] Lambiase F, Paoletti A, Grossi V, Ilio AD. Friction assisted joining of aluminum and PVC sheets. J Manuf Processes 2017;29:221–31.
[49] Lambiase F, Genna S, Kant R. A procedure for calibration and validation of FE modelling of laser-assisted metal to polymer direct joining. Opt Laser Technol 2018;98:363–72.
[50] Lambiase F, Paoletti A, Grossi V, Genna S. Improving energy efficiency in friction assisted joining of metals and polymers. J Mater Process Technol 2017;250:379–89.
[51] Lambiase F, Di Ilio A, Paoletti A. Hybrid numerical modeling of Friction Assisted Joining. J Manuf Processes 2020;57:233–43.
[52] Manente André N, Goushegir SM, Scharnagl N, dos Santos JF, Canto LB, Amancio-Filho ST. Composite surface pre-treatments: Improvement on adhesion mechanisms and mechanical performance of metal–composite friction spot joints with additional film interlayer. The Journal of Adhesion 2018;94(9):723–42.
[53] André NM, Goushegir SM, dos Santos JF, Canto LB, Amancio-Filho ST. Friction Spot Joining of aluminum alloy 2024-T3 and carbon-fiber-reinforced poly (phenylene sulfide) laminate with additional PPS film interlayer: Microstructure, mechanical strength and failure mechanisms. Compos B Eng 2016;94:197–208.
[54] Jiao J, Jia S, Xu Z, Ye Y, Sheng L, Zhang W. Laser direct joining of CFRTP and aluminium alloy with a hybrid surface pre-treating method. Compos B Eng 2019;173:106911.
[55] Mitschang P, Velthuis R, Emrich S, Kopnarski M. Induction heated joining of aluminum and carbon fiber reinforced nylon 66. J Thermoplast Compos Mater 2009;22(6):767–801.
[56] Balle F, Huxhold S, Wagner G, Eifler D. Damage monitoring of ultrasonically welded aluminum/ CFRP-joints by electrical resistance measurements. Proc Eng 2011;10:433–8.